Size and Shape Control of Colloidal Copper(I) Sulfide Nanorods

Marta Kruszynska,[†] Holger Borchert,[†] Alicja Bachmatiuk,[‡] Mark H. Rümmeli,[‡] Bernd Büchner,[‡] Jürgen Parisi,[†] and Joanna Kolny-Olesiak[†,*]

[†]Department of Physics, Energy and Semiconductor Research Laboratory, University of Oldenburg, Carl-von-Ossietzky-Straße 9-11, 26129 Oldenburg, Germany and [‡]Institute for Solid State Research, IFW Dresden, Helmholtzstraße 20, 01069 Dresden, Germany

ABSTRACT Many physical and chemical properties of semiconducting nanocrystals strongly depend on their spatial dimensions and crystallographic structure. For these reasons, achieving a high degree of size and shape control plays an important role with respect to their application potential. In this report we present a facile route for the direct colloidal synthesis of copper(I) sulfide nanorods. A high reactivity of the starting materials is essential to obtain nanorods. We achieve this by using a thiol that thermally decomposes easily and serves as the sulfur source. The thiol is mixed in a noncoordinating solvent, which acts as the reaction medium. Adjustment of the nucleation temperature makes it possible to tailor uniform nanorods with lengths from 10 to 100 nm. The nanorods are single crystalline, and the growth direction is shown to occur along the *a*-axis of djurleite. The growth process and character of the nanorods were investigated through UV–vis and NIR absorption spectroscopy, transmission electron microscopy, and powder X-ray diffraction measurements.

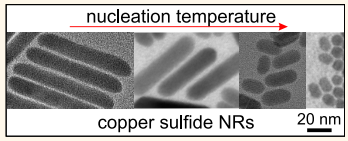

KEYWORDS: copper sulfide · nanocrystals · nanorods · shape control · hot injection

Nanometer-scaled inorganic particles are of significant interest because of their unique size-dependent chemical and physical properties. For these reasons, they are already used in applications in various technological fields, including biological labels,[1,2] light-emitting diodes,[3] and photovoltaic devices.[4–6] Among the family of colloidal semiconductor nanocrystals, much attention has been focused on monodisperse binary chalcogenides, mainly on compounds such as CdS, CdSe, CdTe, PbS, PbSe, and ZnS.[7–10] A disadvantage of many of these materials is the presence of toxic heavy metals. However, there exist other materials that also have promising features, but that have not been very well studied as yet. Of the less studied chalcogenides, an exciting candidate is copper sulfide, which is a p-type semiconducting material with an indirect bulk band gap of ~1.2 eV (for chalcocite) and 1.5 eV (for digenite).[11] Cu–S compounds can occur in a large variety of crystallographic phases with the stoichiometric composition ranging from the copper-rich chalcocite (Cu_2S) to copper-poor villamaninite (CuS_2).[12,13] They are potentially interesting materials for solar cells,[14–16] cold cathodes,[17] and nanoscale switches.[18]

Achieving well-defined size and shape distribution control in colloidal synthesis and the inherent manipulation of the physical and chemical properties of the nanomaterials forming the colloid is challenging, since their final shape and their properties are sensitively inter-related. Thus, the accuracy with which one can tailor such nanostructures limits their application potential.[19,20] In the case of copper sulfide nanocrystals, various reports show the synthesis of spherical particles,[21] polyhedra,[22] hexagonal[23–25] and triangular[26] nanoplates, nanorods (NRs),[27–29] and nanowires.[30] The successful synthesis of copper sulfide nanowires and nanorods has been achieved through the solvent-free thermolysis of copper thiolate precursors, which serve as a kind of template.[30] In some cases, disk-shaped nanocrystals were misinterpreted for nanorods when standing vertically on the substrate.[24,25] The nanorod structures were obtained by first synthesizing cadmium sulfide nanorods followed by the replacement of Cd with Cu using a cation exchange method.[27–29] Up until now, this was the only available method to fabricate copper sulfide nanocrystals with an elongated form (nanorod).

Here, we demonstrate a facile procedure with a high degree of shape and size control for the colloidal synthesis of $Cu_{2-x}S$ nanorods using a classical hot-injection technique. Compared to the above cation exchange method, our experimental procedure is not only straightforward but also environmentally friendly in that no intermediate steps using toxic materials are required.

* Address correspondence to joanna.kolny@uni-oldenburg.de.

Received for review February 1, 2012 and accepted June 19, 2012.

Published online June 19, 2012
10.1021/nn302448n

© 2012 American Chemical Society

RESULTS AND DISCUSSION

In this article we present a synthesis of copper sulfide nanorods (Figure 1) and discuss their growth process. Briefly, copper(I) acetate (CuAc) is dissolved together with trioctylphosphine oxide (TOPO) in 1-octadecene (ODE) at a specific temperature before the sulfur source *tert*-dodecanethiol (*t*-DDT) is injected. After the injection, careful temperature selection enables us to accurately tailor the size and shape of the nanocrystals. At first sight, the similarity of our synthesis procedure to existing literature data[31] appears substantial, but it should be noted that the replacement of 1-dodecanethiol (1-DDT) by *tert*-dodecanethiol in our process plays a crucial role in the successful synthesis of copper sulfide nanocrystals with elongated shape. The length of the nanorods can be easily adjusted between 10 and 100 nm by appropriate temperature selection. We studied the influence of the temperature during the nucleation and growth stages on the shape of the resulting nanorods. Typical schematic examples of temperature profiles used in our study are presented in Figure 1. In the following discussion we use the terms injection, nucleation, and growth temperature to convey the temperature of the copper precursor at the moment of the injection (injection temperature), the temperature of the reaction solution immediately after the injection of *t*-DDT (nucleation temperature), and the final temperature maintained until the end of the reaction (growth temperature).

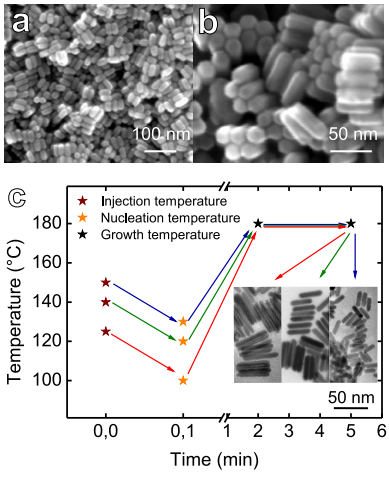

Figure 1. Scanning electron microscopy (SEM) images of copper sulfide nanorods (a and b). Typical examples of the reaction temperature profiles employed for the formation of copper sulfide nanorods with various lengths (c). The inset shows transmission electron microscopy (TEM) images that highlight the variable length of the nanorods.

Typical samples obtained by our synthetic procedure consist of copper sulfide nanorods, which are uniform both in size and in shape (Figure 2a–d). High-resolution transmission electron microscopy (HRTEM) images reveal that the individual nanorods are single crystalline (Figure 3a–c). Spatially resolved energy dispersive X-ray analysis measurements show that the distribution of copper and sulfur atoms within the particles is uniform. We analyzed the images of single particles (Figure 3a–c) in order to determine the growth direction of the nanorods. We always find lattice planes with a distance of 0.34 nm in the growth direction of the nanorods and, depending on the orientation of the particles, lattice plane spacings of 1.35 or 0.19 nm perpendicular to the growth direction. These distances between the lattice planes correspond to djurleite, a monoclinic copper-deficient modification of copper sulfide (a = 26.897 Å, b = 15.745 Å, c = 13.565 Å, $\alpha = \gamma = 90.00°$, $\beta = 90.13°$). The fast Fourier transformation patterns of single particles in various orientations can be indexed to djurleite (Figure 3d–f). The additional superlattice reflections, which can be observed in the patterns, indicate the formation and ordering of defects. The sulfur sublattice of djurleite is hexagonally close-packed with a_{hex} = 0.395 nm and c_{hex} = 0.675 nm. The a-axis of djurleite coincides with

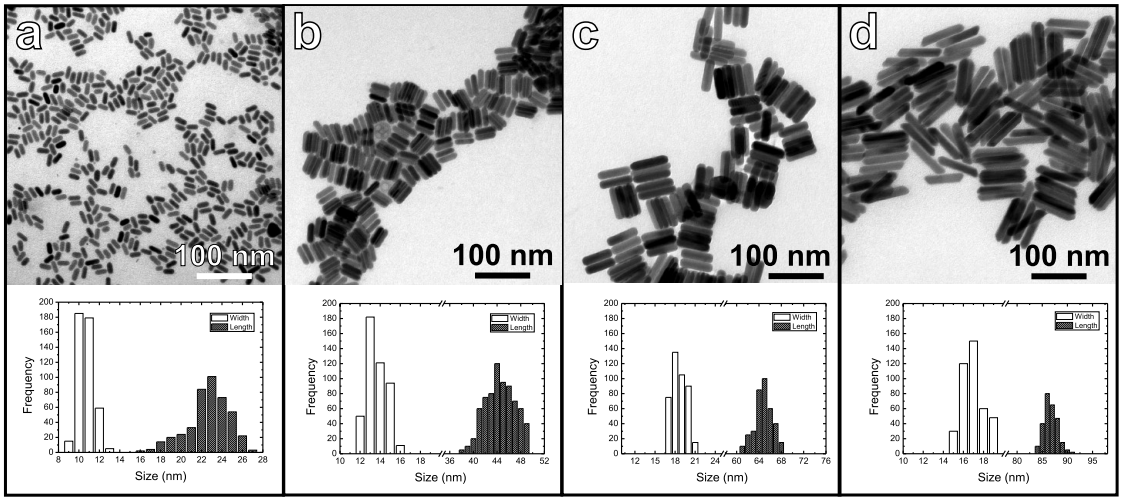

Figure 2. Typical TEM images of nanorods with different length (a–d) together with histograms showing their size distribution.

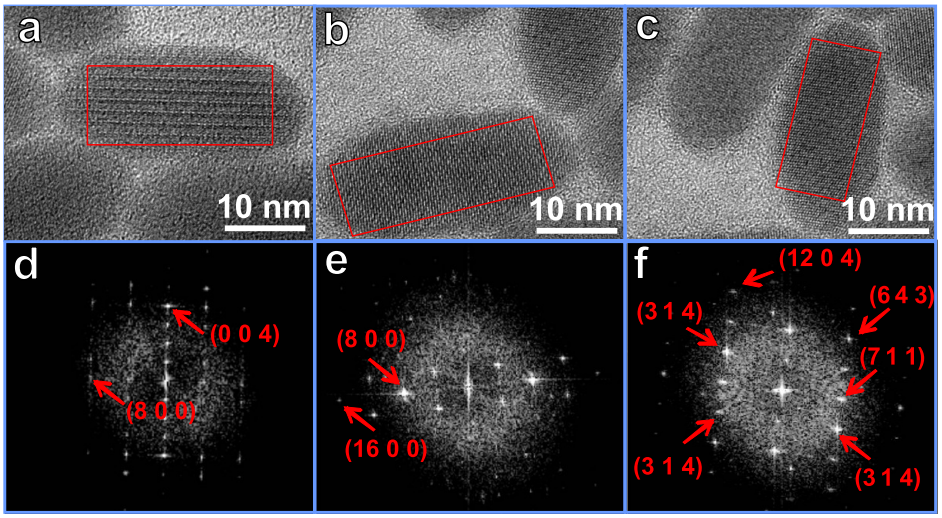

Figure 3. HRTEM analysis of single nanoparticles. (a−c) HRTEM images corresponding to different orientations of the particles on the substrate. (d−f) Fast Fourier transformation of the regions depicted by red rectangles in the TEM images shown above, respectively.

the *c*-axis of this sulfur sublattice. The nanorods grow along the *a*-axis of djurleite, thus, in the direction of the *c*-axis of the sulfur sublattice. It should be noted that the low chalcocite structure is closely related to the djurleite structure; both are based on the same sublattice of sulfur atoms and differ only in the positions of the copper ions; that is, the *c*-axis of the chalcocite lattice coincides with the *c*-axis of the sulfur sublattice. Copper sulfide with a chalcocite structure easily forms nanodisks with (001) planes parallel to the flat surfaces. The latter indicates that these facets are particularly well stabilized under most reaction conditions. In contrast to this, in our synthesis route, the (100) facets (which are equivalent to (001) facets in chalcocite) are the most reactive, and this results in preferential growth along the {100} direction.

To study the growth process of the nanorods, we took aliquots from different reaction times and investigated them with TEM, powder X-ray diffraction (XRD), and UV−vis and NIR absorption spectroscopy. Immediately after the injection of the sulfur source the solution turns yellow and then gradually becomes brown (Figure 4a), indicating the growth of the nanorods. Figure 4b,d,f shows TEM images of nanoparticles obtained from different stages of the reaction, together with their size histograms (Figure 4c,e,g). Initially spherical nanocrystals and some elongated particles with a broad size and shape distribution (aspect ratio 1.2 ± 0.1) are formed (Figure 4b and c); however, they subsequently become more uniform both in size and in shape. Such focusing of the size distribution is an indication of a diffusion-controlled growth process. In the aliquot taken 2 min 30 s after injection, nanorods with an aspect ratio of 2.2 are found (Figure 4d,e). During further growth, their size distribution does not change significantly; however their length increases to 102.4 ± 5.8 nm within 5 min after the injection (Figure 4f,g).

As we see in Figure 5, monodisperse nanocrystals form well-ordered islands of nanorods oriented perpendicular to the substrate. In spite of the fact that the particles have a strong tendency to form an ordered assembly, no long-range order can be observed. The islands consist of tens of hexagonally packed nanorods; however, these islands are randomly oriented with respect to each other. This makes us conclude that the self-assembly might not occur during the drying process on the TEM grid, but could already take place in solution. A closer look at Figure 5a reveals also the presence of some stacks of nanorods oriented parallel to the substrate, which more likely originate from agglomeration in solution than self-assembly on a substrate. Also changes of the absorption properties during the reaction (see discussion below) are in line with this hypothesis.

In order to better investigate the crystallographic structure of the copper sulfide nanocrystals at different stages of the synthesis, XRD patterns were measured for a large number of samples. Some representative examples are presented in Figure 6. As a general remark one should note that copper and sulfur can form a relatively large number of crystallographic phases that often only differ slightly in their exact stoichiometry.[32] Due to the large number of possible phases, the unambiguous assignment of a diffraction pattern to a specific Cu−S phase is not straightforward. Nonetheless, some trends can be extracted from our XRD study. Spherical nanocrystals forming in the early stage of the reaction (two seconds after injection, Figure 6a) were found to correspond to digenite with a Cu:S stoichiometry of 1.8:1. The most intense Bragg reflections observed at 27.7°, 32.1°, 46.0°, and 54.5° are well matched by cubic $Cu_{1.8}S$ (digenite, ICDD numbers 00-056-1256 and 01-072-1966). However, the less intense reflections at 29.7° and 42.3° cannot be explained by the cubic phase. They point to the coexistence

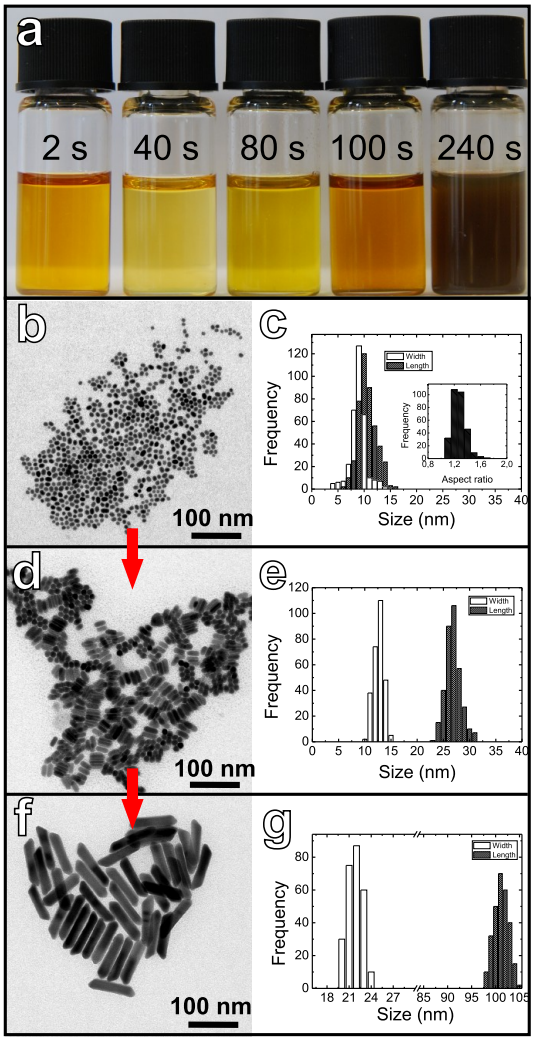

Figure 4. (a) Digital picture of NR solutions obtained at different times after the injection of the sulfur source. The lower panels show TEM images of the copper sulfide nanorods (b, d, f) together with histograms for the width and length (c, e, g). The presented samples represent various stages of the formation of copper sulfide nanocrystals, the growth times being 2:10 min (b, c), 2:30 min (d, e), and 5 min (f, g).

of a rhombohedral modification of digenite (ICDD number 00-023-0962). Note that both structures are closely related. The cubic phase of digenite has a face-centered-cubic (fcc) structure (with a lattice parameter of $a_{cubic} = 5.57$ Å). The fcc structure can, in general, also be described by a rhombohedral (rh) unit cell (with $a = b \neq c$, $\alpha = \beta = 90°$, $\gamma = 120°$). The c-axis is parallel to the diagonal of the cube, and the lattice parameters are related by $a_{rh} = a_{cubic}/\sqrt{2}$ and $c_{rh} = a_{cubic}\sqrt{3}$. In the rhombohedral modification of digenite, the lattice parameters are $a = 3.92$ Å $\approx a_{cubic}/\sqrt{2}$ and $c = 48.8$ Å $\approx 5 \times a_{cubic}\sqrt{3}$. This means that periodicity of the structure along the c-axis is reduced and explains the occurrence of the additional reflections.

After 2 min of growth, the XRD pattern (Figure 6b) does not show any significant change. The XRD pattern

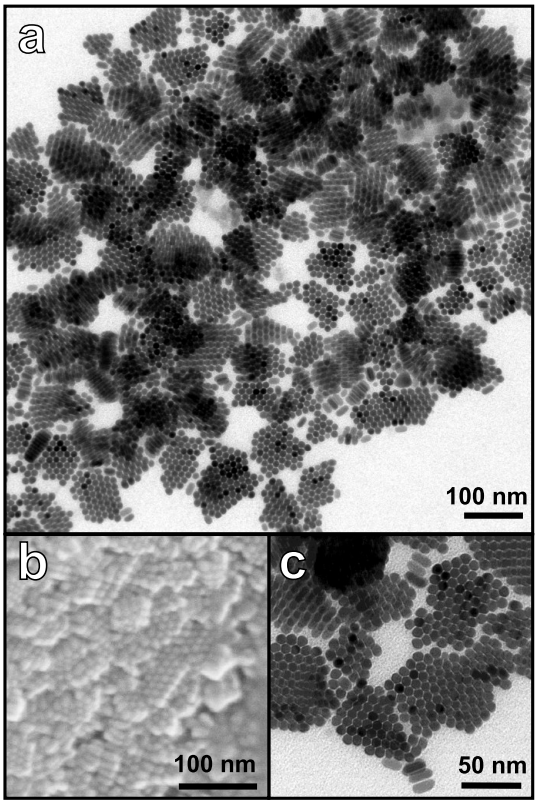

Figure 5. TEM (a, c) and SEM (b) images of self-assembled copper sulfide nanorods.

remains dominated by cubic and rhombohedral modifications of digenite. However, after 2 min 30 s (Figure 6c) considerable changes can be observed. Unfortunately, it was not possible to obtain a good match between the experimental pattern with a single reference pattern from the ICDD database. Djurleite ($Cu_{1.94}S$, ICDD number 00-023-0959) with a Cu:S stoichiometry closer to 2:1 seems to dominate and can explain the most intense reflections. This is in agreement with the HRTEM analysis of individual particles. However, there might also be a contribution from chalcocite (α-Cu_2S, ICDD number 00-002-1294), roxbyite (Cu_7S_4, ICDD number 00-023-0958), or other phases of the Cu−S system. The HRTEM investigations indicate it is unlikely that individual nanocrystals are composed of different phases but that each nanocrystal is a single crystal with a specific structure. However, an ensemble of nanocrystals can contain crystals belonging to different crystallographic phases. In view of the large variety of possible Cu−S phases it is not surprising that the individual crystals of a given sample do not seem to all have exactly the same crystal structure. Independent of the length and width of the nanorods, all examined diffraction patterns consist of peaks located in the same position but have varying relative intensities. We attribute these differences in intensity to the orientation of the nanocrystals on the substrates, *i.e.*, to texture effects. In summary the XRD analysis shows that nanocrystals forming at the beginning of the reaction consist of

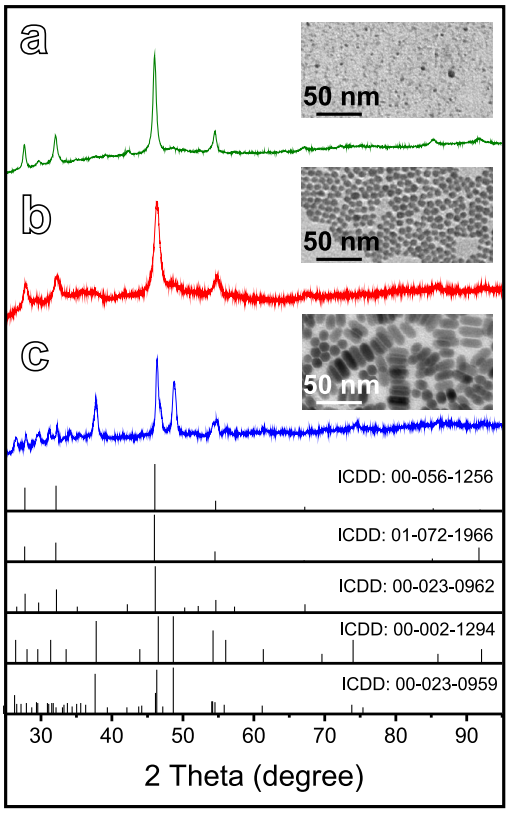

Figure 6. XRD patterns of particles obtained after a reaction time of 2 s (a), 2 min (b), and 2:30 min (c) after the injection of the sulfur source. Reference patterns of cubic digenite ($Cu_{1.8}S$, ICDD numbers 00-056-1256 and 01-072-1966), a rhomohedral modification of digenite ((CDD number 00-023-0962), chalcocite (α-Cu_2S, ICDD number 00-002-1294), and djurleite ($Cu_{1.94}S$, ICDD number 00-023-0959) are shown below the experimental data for comparison.

digenite ($Cu_{1.8}S$). A phase transformation to more copper-rich djurleite ($Cu_{1.94}S$) occurs later.

We now turn to the absorption spectroscopy investigations. Typical UV−vis and NIR absorption spectra of the $Cu_{2-x}S$ NCs are presented in Figure 7. Copper sulfide is an indirect semiconductor, which leads to typical featureless absorption spectra, such as at the beginning of our reaction (*e.g.*, orange curve in Figure 7a). Furthermore, copper sulfide particles show a plasmon resonance, due to their nonstoichiometric composition and the resulting presence of free charge carriers, which is located in the NIR region (Figure 7c).[32,33] The observed changes between the samples extracted after a reaction period between 2 and 100 s can be attributed to the concentration of nanocrystals increasing during the reaction. However, 4 min after the injection (Figure 7a, blue line) the shape of the absorption spectrum changes, with a broad shoulder appearing, which is centered around 460−480 nm. A spectrum with an absorption maximum suggests the presence of a direct gap semiconductor. However, this is not concomitant with the studies on the crystallographic structure of the nanostructures. Thus one can exclude an indirect−direct semiconductor transition arising from individual nanorods. The absorption behavior

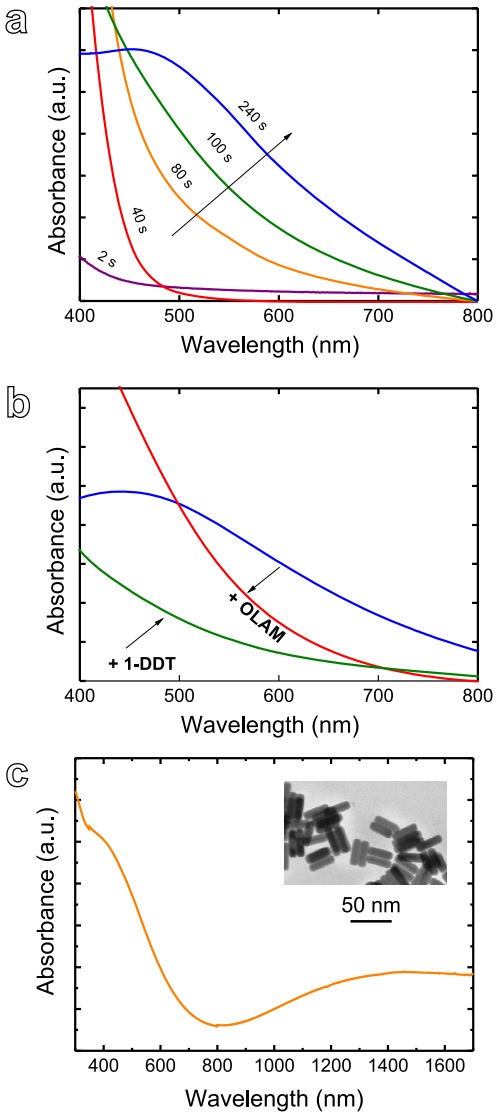

Figure 7. (a) UV−vis absorption spectra of copper sulfide nanocrystals obtained after different reaction times. (b) Changes observed in the absorption spectrum of aggregated nanocrystals (blue line) after the addition of OLAM (red line) and 1-DDT (green line) after and during the synthesis of NRs, respectively. (c) UV−vis−NIR spectrum of copper sulfide nanorods, showing the presence of a plasmon band in the NIR. The inset shows a TEM image of the corresponding sample.

might instead originate from collective phenomena. Indeed, similar changes have been reported previously by Kriegel *et al.*,[34] who attributed the presence of a maximum in the absorption spectrum to the formation of a superlattice of copper sulfide particles. Indirect-semiconductor nanoparticles arranged into a superlattice can form so-called minibands, which leads to a new electronic structure with optically allowed direct transitions.[34,35]

We observe aggregation and even precipitation of the nanorods during the later stages of the synthesis. Also TEM images obtained from solutions, which do not contain a precipitate, give rise to the assumption that the particles can easily form small aggregates (see Figure 5 and discussion above). Thus, we can assign the

changes in the absorption spectra to the formation of some aggregates that are small enough to remain in solution. These aggregates can be broken up or dispersed by the addition of oleylamine,[34] which results in a change of the shape of the absorption spectrum (Figure 7b, red line); namely, it regains the form observed during the first several minutes of the reaction. The recovered spectrum has again the typical form for indirect semiconductors (the maximum disappears). The ability to influence the absorption of copper sulfide through the degree of aggregation could for example be of interest for photovoltaic applications, because a red-shifted spectrum would enable a more efficient exploitation of the solar spectrum. However, from a synthesis perspective, aggregation should be minimized because aggregates can coalesce at elevated temperatures, resulting in a broad size and shape distribution of the products.

In trying to achieve a good stabilization of the nanorods, one should bear in mind that strongly binding ligands can hinder the nanocrystals' one-dimensional growth. In fact, weak stabilization seems to be important for the formation of rod-shaped nanocrystals. Amines and *n*-thiols are common stabilizers for copper sulfide nanocrystals. Nonetheless, both classes of ligands turn out to be unsuitable for the synthesis of nanorods, because they prevent one-dimensional growth. *t*-DDT, which serves as both the sulfur source and stabilizer, is suitable to stabilize the nanorods at the beginning of the reaction. However, its fast thermal decomposition leads to a relatively fast aggregation of the nanorods and subsequent formation of large networks of coalesced particles. This can be avoided by the addition of TOPO. In the concentration range we explored, this additional stabilizer does not influence the size and the shape of the resulting nanorods. It does, though, prolong the time span that the nanorods can grow without aggregation and precipitation. With TOPO, we observe aggregation starting approximately five minutes after the injection of the sulfur source. Therefore, either the growth of copper sulfide nanocrystals has to be stopped before the particles precipitate or a small amount of 1-DDT has to be injected to prevent further aggregation (Figure 7b, green line). The latter step also slows growth.

Stabilizing the surface of nanocrystals can influence their shape and is closely related to the chemical potential of the solution. Molecules that bind to the surface of the nanoparticles can react with the starting materials (*e.g.*, copper ions) and thus control the reactivity and consequently the chemical potential of the reaction solution. Generally, elongated shapes, which are thermodynamically less stable than spheres, form under conditions of high chemical potential. Another prerequisite for the formation of one-dimensional shapes is an intrinsic anisotropy of the crystal structure. The particles with the highly symmetric digenite structure at the beginning of our synthesis are

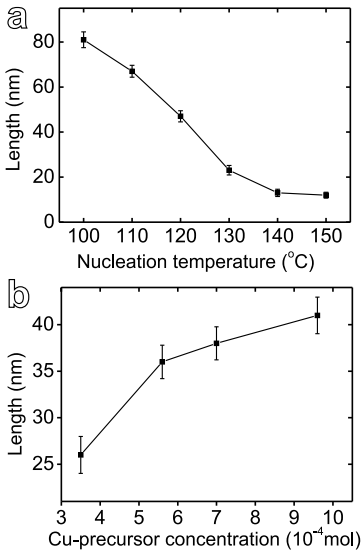

Figure 8. Relationship between the nucleation temperatures and the resulting length of copper sulfide nanorods for a series of comparable reactions (a). Dependence of the length of the nanorods on the concentration of copper monomers (b).

quasi-spherical. It is only after their transformation to the anisotropic djurleite phase that one-dimensional growth starts. The obtained nanorods have either copper- or sulfur-rich (100) facets perpendicular to the growth direction and lateral (010), (001), (011), or higher indexed facets terminated with both copper and sulfur atoms. All these surfaces can be covered by three kinds of ligands: acetate (a weak ligand, introduced into the reaction mixture by the use of copper(I) acetate as the copper source), TOPO (binding more strongly to the surface of copper sulfide, however not influencing the shape of the nanocrystals in control experiments), and *t*-DDT (the strongest of the applied ligands, but decomposing during the reaction). The thermal decomposition of *t*-DDT can take place in solution, but also on the surface of the nanocrystals, which increases their reactivity and growth rate. The latter, together with the high chemical potential of the reaction solution, enables one-dimensional growth of copper sulfide. It is worth noting that replacing *t*-DDT with 1-DDT results in the formation of disk-shaped particles.[31] 1-DDT is more stable at elevated temperatures and thus provides better stabilization for the nanocrystals, while the chemical potential of the solution is lower than with *t*-DDT. Disk-shaped particles are formed as well if we reduce the activity of the copper ions by exchanging the noncoordinating solvent with oleylamine, which can bind to copper ions and, thus, reduce their activity in solution and stabilize copper-rich surfaces on the nanoparticles (Figure S1 in the Supporting Information).

Oleylamine does not influence the rate of the decomposition of *t*-DDT: NMR measurements (Supporting Information, Figure S2) show that *t*-DDT decomposes within several minutes in both solvents (oleylamine and ODE).

Furthermore, chemical reactions between *t*-DDT and the solvents can be excluded. Hence, the observed differences between the reactions in ODE and oleylamine are solely due to the changes in the activity of the copper monomers and the additional stabilization of the nanoparticles by the amine. To summarize, the one-dimensional growth results from an interplay of several factors: the anisotropic crystal structure, high reactivity of the (100) facets of djurleite, and the high reactivity of both the sulfur and the copper monomers in a noncoordinating solvent.

The size of the nanorods can be controlled by changing the reaction conditions. By changing the concentration of the copper monomers one can influence the length of the nanorods. A low concentration of Cu results in the formation of shorter NRs, while longer rods are obtained with higher Cu concentrations (Figure 8b). However, the length control is limited to a narrow range (between *ca*. 25 and 45 nm). This finding motivated us to find other means with which to influence the spatial dimensions of the nanorods. Our studies revealed that the nucleation temperature plays a key role in the growth process and can strongly influence the length of the resulting nanorods. For practical reasons, we varied the injection temperature of *t*-DDT from 120 to 180 °C. The injection of thiols to the reaction solution results in a temperature decrease of approximately 20 °C. This in turn allows nucleation temperature variations between 100 and 160 °C. Control experiments with additional cooling of the reaction solution immediately after the injection showed that the injection temperature itself did not influence the further growth of the nanocrystals. We observed the formation of $Cu_{2-x}S$ nanocrystals only a few seconds after the injection of the sulfur source. However, a reaction temperature of at least 180 °C was necessary for further growth of the copper sulfide nanoparticles. No changes in the reaction solution could be observed below this growth temperature, even with considerably longer reaction times. The longest nanorods formed in the reaction solution at the lowest nucleation temperature (Figure 8a), while higher temperatures led to the formation of NRs with smaller aspect ratios. In contrast to the length of the nanorods, which could be varied between ~15 and ~100 nm, their thickness showed a less pronounced dependence on the reaction conditions (9–23 nm). We attribute this finding to the fact that the nanorods grow from spherical seeds, which regardless of the reaction used have rather similar diameters.

Thus, the factors influencing the growth of the nanorods and their resulting aspect ratio reside in the concentration of the seeds and the resulting availability of the monomers for further growth. Namely, at low nucleation temperatures, the concentration of the seeds and, consequently, the monomer consumption during the seed formation process are lower, as compared to higher temperatures. This results in a higher concentration of the monomers during growth, and thus longer nanorods in reactions with lower nucleation temperatures are formed.

CONCLUSIONS

In summary, copper sulfide nanorods could be synthesized by selecting reaction conditions of high chemical potential. Several factors are crucial to obtaining one-dimensional particle growth. The most important is the use of *tert*-dodecanethiol as the sulfur source, which easily can be decomposed at elevated temperatures and provides the reaction solution with reactive sulfur monomers. Furthermore, the stabilization of the surface of the nanocrystals by *t*-DDT is relatively weak at high temperatures due to its thermal decomposition. This favorably increases the reactivity of the (100) surfaces of the djurleite particles and promotes the nanorod formation. By adjusting the nucleation temperature and copper monomer concentration, control over the length of the nanorods can be achieved.

EXPERIMENTAL SECTION

Synthesis of Copper Sulfide Nanorods. In the synthesis of copper sulfide nanorods, a copper precursor in the form of copper acetate (2 mmol) was dissolved in 1-octadecene (10 mL). Additionally, trioctylphosphine oxide (10 mmol) was added to the reaction. The reaction solution was then stirred under vacuum for 30 min at room temperature. Thereafter, the mixture was placed in a nitrogen atmosphere and heated to 180 °C. While increasing the reaction temperature, the solution color changes from blue-green to yellow-brown, and at this point the sulfur-containing precursor in the form of *tert*-dodecanethiol (7.5 mL) is injected. The injection temperature was varied from 120 to 180 °C, and afterward the temperature was dropped down to 100–160 °C (nucleation temperature). Shortly afterward, the temperature was raised to the growth temperature in the range of 180 °C. The reaction was allowed to proceed between 5 and 10 min. The resulting product was then cooled to room temperature, washed several times with ethanol, and redissolved in hexane for further characterization.

Characterization. UV–vis absorbance spectra of the produced $Cu_{2-x}S$ nanocrystals were measured on a Varian Cary 100 Scan spectrophotometer, and NIR absorbance spectroscopy was recorded on a Varian Cary 5000 Scan spectrophotometer. All the samples for absorption measurements were prepared by diluting 40 μL of the reaction solution with 3 mL of hexane. The samples for TEM investigations were prepared as follows: 20 μL of $Cu_{2-x}S$–hexane solution was dropped onto a standard copper TEM grid and dried at room temperature under ambient conditions. The TEM observations were performed on a Zeiss EM 902A transmission electron microscope with an acceleration voltage of 80 kV. High-resolution TEM images were collected on a double Cs aberration-corrected Jeol 2010F with an electron acceleration voltage of 80 kV. Samples for HRTEM observations were prepared by drop casting the $Cu_{2-x}S$ solution on Formvar-coated gold grids. Samples for SEM prepared by dropping the solution on the Al substrate were investigated with a FEI Helios NanoLab 600i microscope. Powder X-ray diffraction was measured with a PANalyticalX'Pert PRO MPD diffractometer operating with Cu Kα radiation and Bragg–Brentano θ–2θ

geometry. The samples were measured on low-background silicon sample holders and prepared for the XRD measurements as follows: Nanocrystals in hexane solution were dropped on the silicon substrate and heated to 70 °C for 30 min, in order to remove the solvent.

Conflict of Interest: The authors declare no competing financial interest.

Acknowledgment. We gratefully acknowledge funding of the EWE Research Group "Thin Film Photovoltaics" by the EWE AG, Oldenburg. We thank Karsten von Maydell for the possibility of conducting UV–vis–NIR measurements. A.B. thanks the Alexander von Humboldt Foundation and the BMBF. M.H.R. thanks the EU (ECEMP) and the Freistaat Sachsen.

Supporting Information Available: TEM image of copper sulfide nanodisks synthesized with *t*-DDT in oleylamine, NMR analysis of the decomposition of *t*-DDT in oleylamine and octadecene, and characterization of the reaction solution before the injection of the sulfur source. This material is available free of charge *via* the Internet at http://pubs.acs.org.

REFERENCES AND NOTES

1. Li, L.; Daou, T. J.; Texier, I.; Kim Chi, T. T.; Liem, N. Q.; Reiss, P. Highly Luminescent $CuInS_2$/ZnS Core/Shell Nanocrystals: Cadmium-Free Quantum Dots for *in Vivo* Imaging. *Chem. Mater.* **2009**, *21*, 2422–2429.
2. Derfus, A. M.; Chan, W. C. W.; Bhatia, S. N. Intracellular Delivery of Quantum Dots for Live Cell Labeling and Organelle Tracking. *Adv. Mater.* **2004**, *16*, 961–966.
3. Rogach, A. L.; Gaponik, N.; Lupton, J. M.; Bertoni, C.; Gallardo, D. E.; Dunn, S.; Pira, N. Li; Paderi, M.; Repetto, P.; *et al*. Light-Emitting Diodes with Semiconductor Nanocrystals. *Angew. Chem., Int. Ed.* **2008**, *47*, 6538–6549.
4. Zhou, Y.; Eck, M.; Krüger, M. Bulk-Heterojunction Hybrid Solar Cells Based on Colloidal Nanocrystals and Conjugated Polymers. *Energy Environ. Sci.* **2010**, *3*, 1851–1864.
5. Borchert, H. Elementary Processes and Limiting Factors in Hybrid Polymer/Nanoparticle Solar Cells. *Energy Environ. Sci.* **2010**, *3*, 1682–1694.
6. Xu, T.; Qiao, Q. Conjugated Polymer–Inorganic Semiconductor Hybrid Solar Cells. *Energy Environ. Sci.* **2011**, *4*, 2700–2720.
7. Peng, Z. A.; Peng, X. G. Formation of High-Quality CdTe, CdSe, and CdS Nanocrystals Using CdO as Precursor. *J. Am. Chem. Soc.* **2001**, *123*, 183–184.
8. Joo, J.; Na, H. B.; Yu, T.; Yu, J. H.; Kim, Y. W.; Wu, F. X.; Zhang, J. Z.; Hyeon, T. Generalized and Facile Synthesis of Semiconducting Metal Sulfide Nanocrystals. *J. Am. Chem. Soc.* **2003**, *125*, 11100–11105.
9. Alivisatos, A. P. Semiconductor Clusters, Nanocrystals, and Quantum Dots. *Science* **1996**, *271*, 933–937.
10. Jin, X.; Kruszynska, M.; Parisi, J.; Kolny-Olesiak, J. Catalyst-Free Synthesis and Shape Control of CdTe Nanowires. *Nano Res.* **2011**, *4*, 824–835.
11. Mulder, B. J. Optical Properties of Crystals of Cuprous Sulphides (Chalcosite, Djurleite, $Cu_{1.9}S$, and Digenite). *Phys. Status Solidi A* **1972**, *13*, 79–88.
12. Isac, L.; Duta, A.; Kriza, A.; Manolache, S.; Nanu, M. Copper Sulfides Obtained by Spray Pyrolysis-Possible Absorbers in Solid-State Solar Cells. *Thin Solid Films* **2007**, *515*, 5755–5758.
13. Ueda, H.; Nohara, M.; Kitazawa, K.; Takagi, H.; Fujimori, A.; Mizokawa, T.; Yagi, T. Copper Pyrites CuS_2 and $CuSe_2$ as Anion Conductors. *Phys. Rev. B* **2002**, *65*, 155104.
14. Lee, H.; Yoon, S. W.; Kim, E. J.; Park, J. *In-Situ* Growth of Copper Sulfide Nanocrystals on Multiwalled Carbon Nanotubes and Their Application as Novel Solar Cell and Amperometric Glucose Sensor Materials. *Nano Lett.* **2007**, *7*, 778–784.
15. Wu, Y.; Wadia, C.; Ma, W.; Sadtler, B.; Alivisatos, A P. Synthesis and Photovoltaic Application of Copper(I) Sulfide Nanocrystals. *Nano Lett.* **2008**, *8*, 2551–2555.
16. Page, M.; Niitsoo, O.; Itzhaik, Y.; Cahen, D.; Hodes, G. Copper Sulfide as a Light Absorber in Wet-Chemical Synthesized Extremely Thin Absorber (ETA) Solar Cells. *Energy Environ. Sci.* **2009**, *2*, 220–223.
17. Chen, J.; Deng, S. Z.; Xu, N. S.; Wang, S. H.; Wen, X. G.; Yang, S. H.; Yang, C. L.; Wang, J. N.; Ge, W. K. Field Emission from Crystalline Copper Sulphide Nanowire Arrays. *Appl. Phys. Lett.* **2002**, *80*, 3620–3622.
18. Chen, L.; Xia, Y. D.; Liang, X. F.; Yin, K. B.; Yin, J.; Liu, Z. G.; Chen, Y. Nonvolatile Memory Devices with Cu_2S and Cu-Pc Bilayered Films. *Appl. Phys. Lett.* **2007**, *91*, 073511.
19. Xie, R.; Rutherford, M.; Peng, X. Formation of High-Quality I–III–VI Semiconductor Nanocrystals by Tuning Relative Reactivity of Cationic Precursors. *J. Am. Chem. Soc.* **2009**, *131*, 5691–5697.
20. Jun, Y.; Choi, J.; Cheon, J. Shape Control of Semiconductor and Metal Oxide Nanocrystals through Nonhydrolytic Colloidal Routes. *Angew. Chem., Int. Ed.* **2006**, *45*, 3414–3439.
21. Li, S.; Wang, H.; Xu, W.; Si, H.; Tao, X.; Lou, S.; Du, Z.; Li, L. S. Synthesis and Assembly of Monodisperse Spherical Cu_2S Nanocrystals. *J. Colloid Interface Sci.* **2009**, *330*, 483–487.
22. Li, W.; Shavel, A.; Guzman, R.; Rubio-Garcia, J.; Flox, C.; Fan, J.; Cadavid, D.; Ibáñez, M.; Arbiol, J.; Morante, J. R.; Cabot, A. Morphology Evolution of $Cu_{2-x}S$ Nanoparticles: From Spheres to Dodecahedrons. *Chem. Commun.* **2011**, *47*, 10332–10334.
23. Li, X.; Shen, H.; Niu, J.; Li, S.; Zhang, Y.; Wang, H.; Li, L. S. Columnar Self-Assembly of Cu_2S Hexagonal Nanoplates Induced by Tin (IV)-X Complex as Inorganic Surface Ligand. *J. Am. Chem. Soc.* **2010**, *132*, 12778–12779.
24. Sigman, M. B., Jr.; Ghezelbash, A.; Hanrath, T.; Saunders, A. E.; Lee, F.; Korgel, B. A. Solventless Synthesis of Monodisperse Cu_2S Nanorods, Nanodisks, and Nanoplatelets. *J. Am. Chem. Soc.* **2003**, *125*, 16050–16057.
25. Larsen, T. H.; Sigman, M.; Ghezelbash, A.; Doty, R. C.; Korgel, B. A. Solventless Synthesis of Copper Sulfide Nanorods by Thermolysis of a Single Source Thiolate-Derived Precursor. *J. Am. Chem. Soc.* **2003**, *125*, 5638–5639.
26. Lou, W. J.; Chen, M.; Wang, X. B.; Liu, W. M. Size Control of Monodisperse Copper Sulfide Faceted Nanocrystals and Triangular Nanoplates. *J. Phys. Chem. C* **2007**, *111*, 9658–9663.
27. Luther, J. M.; Zheng, H. M; Sadtler, B.; Alivisatos, A. P. Synthesis of PbS Nanorods and Other Ionic Nanocrystals of Complex Morphology by Sequential Cation Exchange Reactions. *J. Am. Chem. Soc.* **2009**, *131*, 16851–16857.
28. Sadtler, B.; Demchenko, D. O.; Zheng, H.; Hughes, S. M.; Merkle, M. G.; Dahmen, U.; Wang, L. W.; Alivisatos, A. P. Selective Facet Reactivity during Cation Exchange in Cadmium Sulfide Nanorods. *J. Am. Chem. Soc.* **2009**, *131*, 5285–5293.
29. Rivest, J. B.; Fong, L. M.; Jain, P. K.; Toney, M. F.; Alivisatos, A. P. Size Dependence of a Remperature-Induced Solid-Solid Phase Transition in Copper(I) Sulfide. *J. Phys. Chem. Lett.* **2011**, *2*, 2402–2406.
30. Chen, L.; Chen, Y. B.; Wu, L. M. Synthesis of Uniform Cu_2S Nanowires from Copper-Thiolate Polymer Precursors by a Solventless Thermolytic Method. *J. Am. Chem. Soc.* **2004**, *126*, 16334–16335.
31. Wang, Y.; Hu, Y.; Zhang, Q.; Ge, J.; Lu, Z.; Hou, Y.; Yin, Y. One-Pot Synthesis and Optical Property of Copper(I) Sulfide Nanodisks. *Inorg. Chem.* **2010**, *49*, 6601–6608.
32. Zhao, Y.; Pan, H.; Lou, Y.; Qiu, X.; Zhu, J.; Burda, C. Plasmonic $Cu_{2-x}S$ Nanocrystals: Optical and Structural Properties of Copper-Deficient Copper(I) Sulfides. *J. Am. Chem. Soc.* **2009**, *131*, 4253–4261.
33. Luther, J. M.; Jain, P. K.; Ewers, T.; Alivisatos, P. Localized Surface Plasmon Resonances Arising from Free Carriers in Doped Quantum Dots. *Nat. Mater.* **2011**, *10*, 361–366.
34. Kriegel, I.; Rodríguez-Fernández, J.; Como, E. D.; Lutich, A. A.; Szeifert, J. M.; Feldmann, J. Tuning the Light Absorption of $Cu_{1.97}S$ Nanocrystals in Supercrystal Structures. *Chem. Mater.* **2011**, *23*, 1830–1834.
35. Gnutzmann, U.; Clausecker, K. Theory of Direct Aptical Transitions in an Optical Indirect Semiconductor with a Superlattice Structure. *Appl. Phys.* **1974**, *3*, 9–14.